



## Hybrid smoothed finite element method for two-dimensional underwater acoustic scattering problems



Yingbin Chai<sup>a</sup>, Wei Li<sup>a,b,c,\*</sup>, Zhixiong Gong<sup>a</sup>, Tianyun Li<sup>a,b,c</sup>

<sup>a</sup> School of Naval Architecture and Ocean Engineering, Huazhong University of Science and Technology, Wuhan, Hubei 430074, China

<sup>b</sup> Hubei Key Laboratory of Naval Architecture & Ocean Engineering Hydrodynamics (HUST), Wuhan, Hubei 430074, China

<sup>c</sup> Collaborative Innovation Center for Advanced Ship and Deep-Sea Exploration (CISSE), Shanghai 200240, China

### ARTICLE INFO

#### Article history:

Received 21 March 2015

Accepted 22 February 2016

Available online 5 March 2016

#### Keywords:

Hybrid smoothed finite element method (HS-FEM)

Dirichlet-to-Neumann (DtN) condition

Unbounded domain

Underwater acoustic scattering

Numerical methods

### ABSTRACT

It is well known that the standard finite element method (FEM) is unreliable to solve acoustic problems governed by the Helmholtz equation with large wave numbers due to the “overly-stiff” nature of the FEM. In order to overcome this shortcoming, the hybrid smoothed finite element method (HS-FEM) using triangular elements is presented for the two-dimensional underwater acoustic scattering problems. In the HS-FEM, a scale factor  $\alpha \in [0, 1]$  is introduced to establish the area-weighted gradient field that contains contributions from both the standard FEM and the node-based smoothed finite element method (NS-FEM). The HS-FEM can provide a close-to-exact stiffness of the continuous system, thus the numerical dispersion error can be significantly decreased. To handle the underwater acoustic scattering problems in an infinite fluid medium, the bounded computational domain is obtained by introducing an artificial boundary on which the Dirichlet-to-Neumann (DtN) condition is imposed. Several numerical examples are investigated and the results showed that HS-FEM can provide more accurate solutions than the standard FEM. Therefore, the present method can be applied to practical underwater acoustic scattering problems such as sonar mine-hunting and sonar detection in ocean acoustics.

© 2016 Elsevier Ltd. All rights reserved.

## 1. Introduction

In the past several decades, the time-harmonic acoustic problems in a homogeneous medium governed by the Helmholtz equation have been a very active research field. In general, the acoustic problems can be classified into interior and exterior problems. Due to limitations of the analytical method, the analytical solutions are only available for very simple geometries. Thus the numerical methods are of great importance in solving these acoustic problems with complex geometries.

One popular and powerful numerical method for coping with the time-harmonic acoustic problems is the standard finite element method (FEM). There is a great deal of relevant research work which can be found in the published literatures (Crocker, 1975; Petyt et al., 1976; Nefske et al., 1982; Harari and Magoulès, 2004). However, the numerical approaches for handling the acoustic problems still remain two major challenges. The first challenge is how to treat the exterior acoustic problems in unbounded domains effectively. Initially, the FEM was applied to

acoustics with the aim of solving the interior problems in bounded domains. For exterior problems, including acoustic radiation and scattering, the well-known Sommerfeld radiation condition should be satisfied so that there is no spurious wave reflected from the far field. Another challenge is the numerical dispersion issue (Ihlenburg and Babuška, 1995, 1997; Ihlenburg et al., 1997; Deraemaeker et al., 1999). In general, the numerical methods can obtain relatively accurate results in the low frequency range. However, with the increase of the frequency, the numerical dispersion error will increase dramatically.

In order to use the FEM for exterior acoustic problems, the unbounded domain is usually truncated by an artificial boundary on which the non-reflecting boundary condition is imposed to replace the Sommerfeld radiation condition at infinity. In recent years, a series of numerical treatments including absorbing boundary conditions (Engquist and Majda, 1977; Clayton and Engquist, 1977; Higdon, 1987; Hu, 2004), Dirichlet to Neumann (DtN) boundary conditions (Keller and Givoli, 1989; Harari et al., 1998; Grote and Kirsch, 2004; Givoli et al., 1998) and perfectly matched layer (PML) (Hastings et al., 1996; Berenger, 1994; Turkel and Yefet, 1998) have been proposed to handle exterior acoustic problems. Among them the DtN boundary condition devised by Givoli and Keller is an exact non-reflecting boundary condition. It relates the “Dirichlet datum” to the “Neumann datum” with the

\* Corresponding author at: School of Naval Architecture and Ocean Engineering, Huazhong University of Science and Technology, Wuhan, Hubei 430074, China.

E-mail address: [hustliw@hust.edu.cn](mailto:hustliw@hust.edu.cn) (W. Li).

help of an integral operator. Although this boundary condition is non-local, it still possesses high computational efficiency and can obtain much more accurate results than those obtained from various approximate local conditions. Therefore, many researchers have applied the DtN boundary conditions to cope with all kinds of exterior acoustic problems and other problems in large finite domains.

For the purpose of reducing the numerical dispersion error in acoustic problems, various numerical techniques based on the standard finite element method have been developed to tackle this issue, such as the Galerkin/least-squares finite element method (GLS) (Harari and Hughes, 1992; Harari and Nogueira, 2002; Thompson and Pinsky, 1995), the quasi-stabilized finite element method (QSFEM) (Deraemaeker et al., 1999) and the residual-free finite element method (RFEM) (Franca et al., 1997). However, all of the above methods can not reduce the numerical dispersion error effectively.

In addition to the standard finite element method and the extended finite element method, the meshfree methods have been also introduced to solve the acoustic problems. Belytschko et al. (1994) proposed the element-free Galerkin method (EFGM) to tackle the numerical dispersion in acoustic problems. Bouillard and Suleaub (2008) found that the EFGM is effective to reduce the numerical dispersion error significantly compared to the FEM even though the EFGM also suffers from the dispersion and pollution effect. However, in order to control the numerical dispersion error, delicate background cells and a large number of quadrature points are needed for the global numerical integration, leading to prohibitive computational demands. As mentioned in He et al. (2009), the approximate discrete model is the main reason to cause dispersion error. The stiffness of the discretized model obtained from the standard FEM always behaves stiffer than the original model, leading to the so-called numerical dispersion error. So producing a properly “softened” stiffness for the discrete model is much more essential to control the numerical error. Recently, Liu et al. (2007a, 2007b, 2009) have proposed a series of smoothed finite element methods (S-FEM) which are formulated by incorporating the strain smoothing techniques of meshfree methods into the existing standard finite element methods (Li et al., 2014a, 2014b). Because the S-FEM always provide “softer” models than the standard FEM owing to the smoothing techniques, this makes the S-FEM models can achieve more accurate numerical solutions than the FEM models.

In recent years, the S-FEM have been introduced to solve the acoustic problems and coupled structural-acoustic problems (He et al., 2010b, 2011a, 2011b, 2012; Li et al., 2014a, 2014b) and it is found that S-FEM is more effective to control the numerical error than the standard FEM. The present paper is inspired by the work Li et al. (2015) on hybrid smoothed finite element method (HS-FEM) for acoustic problems. This work mainly focused on interior acoustic problems or coupling of structural acoustic problems. As an extension of this, the aim of the current research is to address the problem of scattering of acoustic wave from infinite cylinders in water. In fact, there is a great deal of relevant research can be found in the literatures. Initially, researchers tried to solve the problem mentioned above using analytical method and the geometry of the scatter was also restricted to circular cylinders. Actually, the exact solutions are available only for the scatter with simple geometry. When it comes to more complex and more realistic scatter, one have to resort to numerical methods. Pillai et al. (1982) utilized the T-matrix method to handle the sound scattering by rigid and elastic infinite elliptical cylinder in water. DiPerna and Stanton (1994) derived a conformal mapping approach for solving sound scattering by cylinders of non-circular cross section. Recently, Mitri (2015a, 2015b, 2016) used the partial-wave series expansion (PWSE) method to calculate the acoustic scattering and radiation force on a rigid elliptical cylinder in different waves. In addition, some other numerical techniques such as the mode matching method (MMM) (Ikuno and Yasuura, 1978), the Fourier

matching method (FMM) (DiPerna and Stanton, 1994), the boundary element method (BEM) (Seybert et al., 1988) and the finite element method (FEM) (Strouboulis et al., 2008) have also been developed to tackle this issue with varying degree of success.

In this paper, the HS-FEM was combined with the DtN boundary condition to give a HS-FEM-DtN model for sound scattering by infinitely long rigid cylinders in water. Both circular and noncircular cross sections are considered in current research. Due to the good performance of the HS-FEM in interior acoustic problems, it is expected that the HS-FEM will solve the exterior acoustic problems with very exact solutions.

This paper is organized as follows: Section 2 introduces the finite element formulation for exterior acoustic problems in unbounded domains. Section 3 briefly describes the Dirichlet to Neumann boundary condition for finite element schemes. Section 4 contains the detailed formulation of the hybrid smoothed finite element method. Dispersion error analysis of acoustic problems using HS-FEM is presented in Section 5. Section 6 outlines the numerical error for acoustic problems. In Section 7, several numerical examples are studied in details. Final conclusions from the numerical results are drawn in Section 8.

## 2. The finite element formulation for exterior acoustic problems in unbounded domains

As shown in Fig. 1, an exterior acoustic problem in an infinite domain  $R$  bounded internally by the surface  $\Gamma$  of an obstacle is considered. We assume that the boundary  $\Gamma$  can be decomposed into two portions Dirichlet boundary condition  $\Gamma_p$  and Neumann boundary condition  $\Gamma_v$ , where  $\Gamma = \Gamma_p \cup \Gamma_v$  and  $\Gamma_p \cap \Gamma_v = \emptyset$ .

The exterior boundary-value problem can be described in the following equations.

$$\Delta p + k^2 p + f = 0 \quad \text{in } R \quad (1)$$

$$p = g \quad \text{on } \Gamma_g \quad (2)$$

$$\nabla u \cdot n = h \quad \text{on } \Gamma_h \quad (3)$$

here  $p$  denotes the spatial part of the acoustic pressure or velocity potential,  $\Delta$  and  $k$  represent the Laplace operator and wave number, respectively,  $f$ ,  $g$  and  $h$  are given functions.

For exterior acoustic problem in unbounded domains, the Sommerfeld radiation condition which requires only outgoing waves be proportional to  $\exp(ikr)$  at infinity. The radiation condition requires that energy flux be positive at infinity, this property guarantees that the boundary-value problem has unique solution.

The Sommerfeld radiation condition can be describe as follows:

$$\lim_{r \rightarrow \infty} r^{\frac{(d-1)}{2}} \left( \frac{\partial p}{\partial r} - ikp \right) = 0 \quad (4)$$

where  $d$  is the spatial dimension.

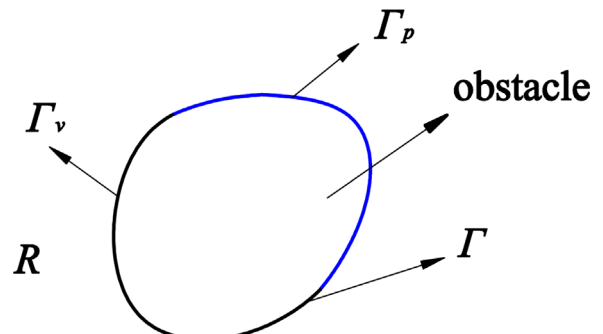
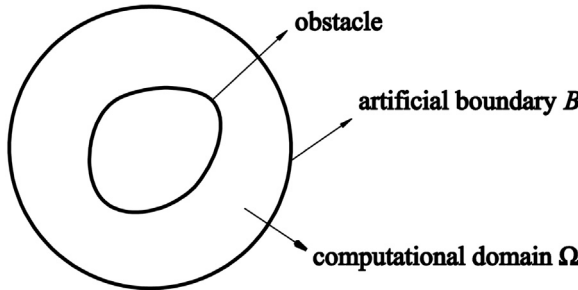


Fig. 1. The exterior acoustic problem in an infinite domain.



**Fig. 2.** The infinite domain is usually truncated by an artificial boundary  $B$  yielding a finite computational domain  $\Omega$ .

In order to solve the exterior acoustic problem using numerical method, the infinite domain is usually truncated by an artificial boundary  $B$  yielding a finite computational domain  $\Omega$ . As shown in Fig. 2, on  $B$  the well-known Dirichlet to Neumann (DtN) map is imposed to replace the Sommerfeld radiation condition at infinity. Then (Eqs. (1) and 4) can be written in the following form:

$$\nabla^2 p + k^2 p + f = 0 \quad \text{in } \Omega \quad (5)$$

$$p_v = -Mp \quad \text{on } B \quad (6)$$

where  $M$  denotes the DtN operator which relating the Dirichlet datum  $p$  to the Neumann datum  $p_v$  on  $B$ .

To construct the weak form of the above problem, two function spaces are defined as follows:

$$s = \left\{ p \mid p \in H^1(\Omega) \text{ and } p = g \text{ on } \Gamma_g \right\} \quad (7)$$

$$s_0 = \left\{ w \mid w \in H^1(\Omega) \text{ and } w = 0 \text{ on } \Gamma_g \right\} \quad (8)$$

where  $H'$  is the first order Sobolev space given by

$$H^1(\Omega) = \left\{ \psi(x) \mid \psi \in L_2(\Omega), \frac{\partial \psi}{\partial x_i} \in L_2(\Omega) \right\} \quad (9)$$

Then the equivalent problem is to find  $p \in s$  such that for all  $w \in s_0$

$$a(w, p) + b(w, p) = (p, f) + (w, h)_\Gamma \quad (10)$$

Eq. (10) is the weak form of this problem and

$$a(w, p) = \int_{\Omega} (\nabla w \cdot \nabla p - k^2 w p) d\Omega = 0 \quad (11)$$

$$b(w, p) = \int_B w M p d\mathcal{B} \quad (12)$$

$$(w, f) = \int_{\Omega} w f d\Omega \quad (13)$$

$$(w, h)_\Gamma = \int_{\Gamma_h} w h d\Gamma \quad (14)$$

In order to obtain the finite element spaces  $s$  and  $s_0$  using the Galerkin finite element method, the computational domain  $\Omega$  is discretized into a finite number of elements.  $\eta_g$  is defined to be the set of all the nodes on the boundary  $\Gamma_g$  in which  $p$  is known and  $\eta$  is defined to be the set of all the other nodes where the value of  $p$  is unknown. Then the functions  $p^h$  and  $w^h$  can be expressed in the approximate form:

$$p^h(\mathbf{x}) = \sum_{A \in \eta} d_A N_A(\mathbf{x}) + \sum_{A \in \eta_g} g_A N_A^g(\mathbf{x}) \quad (15)$$

$$g_A = g(\mathbf{x}_A) \quad \text{for } A \in \eta_g \quad (16)$$

$$w^h(\mathbf{x}) = \sum_{A \in \eta} c_A N_A(\mathbf{x}) \quad (17)$$

where  $N_A$  is the defined shape function for each node  $A \in \eta$  and  $N_A^g$  is the defined shape function for each node  $A \in \eta_g$ ,  $d_A$  and  $c_A$  are constants and  $\mathbf{x}_A$  is the coordinate at node  $A$ .

Substituting (Eqs. (15) and 17) into Eq. (10), the discretized system equations for exterior acoustic problem can be obtained as:

$$\mathbf{Kp} = \mathbf{F} \quad (18)$$

where  $\mathbf{K}$  is the system stiffness matrix,  $\mathbf{p}$  is the unknown nodal acoustic pressure in the computational domain,  $\mathbf{F}$  is the vector of nodal force.

The system stiffness matrix  $\mathbf{K}$  can be written as:

$$\mathbf{K} = \mathbf{K}^a + \mathbf{K}^b \quad (19)$$

where

$$\mathbf{K}^a = [\mathbf{K}_{IJ}^a] \quad \mathbf{K}^b = [\mathbf{K}_{IJ}^b] \quad (20)$$

$$\mathbf{K}_{IJ}^a = a(N_I, N_J) = \int_{\Omega} (\nabla \mathbf{N})^T \nabla \mathbf{N} d\Omega - k^2 \int_{\Omega} \mathbf{N}^T \mathbf{N} d\Omega \quad (21)$$

$$\mathbf{K}_{IJ}^b = b(N_I, N_J) \quad (22)$$

where  $I$  and  $J$  denote the node number and  $N_I$  is the defined shape function for node  $I$ .

It can be seen from Eq. (19) that the effect of the DtN boundary condition on the standard finite element method is the inclusion of the matrix  $\mathbf{K}^b$  in the system stiffness  $\mathbf{K}$ . Due to the local support property of the FEM shape functions, the value of  $N_I$  equals 1 at node  $I$  and equals 0 at every other node. Besides,  $N_I$  will vanish outside a local patch of elements which share node  $I$ . Then the matrix  $\mathbf{K}_{IJ}^b$  is nonzero only if both nodes  $I$  and  $J$  lie on the boundary  $B$ .

### 3. The Dirichlet to Neumann boundary condition for finite element schemes

In this section, we will derive explicit expressions of the DtN map  $M$ . Initially, the infinite domain is divided into two sub-domains by an artificial boundary  $\Gamma_R$  (see Fig. 1), which is generally a circle or sphere of radius  $R$ . Then the original problem is equivalent to sub-problems. They are called sub-problem  $O$  and sub-problem  $I$ .

Sub-problem  $O$  in the unbounded domain can be described as the radiation problem of a circle or sphere and it is governed by (Eqs. (1) and 4).

According to Keller and Givoli (1989), the exact solution of the sub-problem  $O$  in two dimensions can be expressed as:

$$p(r, \theta) = \frac{1}{\pi} \sum_{n=0}^{\infty} \int_0^{2\pi} \frac{H_n^{(1)}(kr)}{H_n^{(1)}(kR)} \cos n(\theta - \theta') p(R, \theta') d\theta' \quad (23)$$

where  $p(r, \theta)$  denotes the unknown value of the acoustic pressure. The prime after the sum indicates that a factor of 1/2 multiplies the term with  $n = 0$ .  $H_n^{(1)}$  represents the Hankel function of the first kind.

Then the normal derivative of the acoustic pressure  $p_v$  on the artificial boundary can be obtained as:

$$p_v = \frac{\partial p(r, \theta)}{\partial n} \Big|_{r=R} = - \sum_{n=0}^{\infty} \int_0^{2\pi} m_n(\theta - \theta') p(R, \theta') d\theta' \quad (24)$$

where

$$m_n(\theta - \theta') = -\frac{k}{\pi} \frac{H_n^{(1)\prime}(kR)}{H_n^{(1)}(kR)} \cos n(\theta - \theta') \quad (25)$$

Here  $m_n(\theta - \theta')$  is the DtN kernels and it can be separated as

$$m_n(\theta - \theta') = -\frac{k H_n^{(1)}(kR)}{\pi H_n^{(1)}(kR)} (\cos n\theta \cos n\theta' + \sin n\theta \sin n\theta') \quad (26)$$

By substituting Eq. (24) and Eq. (23) into Eq. (6), the stiffness matrix  $\mathbf{K}^b$  which contains the DtN operator  $M$  can be obtained as:

$$\begin{aligned} K_{IJ}^b &= b(N_I, N_J) = \int_B N_I M N_J d\Omega \\ &= -\sum_{j=0}^{\infty} \frac{k H_n^{(1)}(kr)}{\pi H_n^{(1)}(kR)} \left( \int_B N_I(\mathbf{x}) F_j(\mathbf{x}) d\Omega \right) \left( \int_B N_J(\mathbf{x}) F_j(\mathbf{x}') d\Omega \right) \end{aligned} \quad (27)$$

where the simple trigonometric functions  $F_j(\mathbf{x})$  and  $F_j(\mathbf{x}')$  are determined by:

$$F_j(\mathbf{x}) = [\cos n\theta \quad \sin n\theta] \quad (28)$$

$$F_j(\mathbf{x}') = \begin{bmatrix} \cos n\theta' \\ \sin n\theta' \end{bmatrix} \quad (29)$$

The matrix  $K_{IJ}^b$  corresponds to DtN boundary condition, after having calculated  $K_{IJ}^b$ , the exterior acoustic problems in unbounded domain can be solved by the standard finite element scheme.

#### 4. Formulation of the hybrid smoothed finite element method (HS-FEM)

##### 4.1. The node-based smoothed finite element method (NS-FEM) for acoustic problems

In the NS-FEM model, the problem domain  $\Omega$  is first divided into  $N_e$  elements with  $N_n$  nodes, such that  $\Omega = \sum_{i=1}^{N_e} \Omega_i^e$  and  $\Omega_i^e \cap \Omega_j^e = \emptyset, i \neq j$ , as in the standard FEM. The generated elements can be polygons with arbitrary number of sides and used as background elements in the NS-FEM. On the top of the background element mesh, the problem domain  $\Omega$  is further divided into  $N_n$  smoothing domains associated with nodes of the polygonal elements such that  $\Omega = \sum_{i=1}^{N_n} \Omega_i^s$  and  $\Omega_i^s \cap \Omega_j^s = \emptyset, i \neq j$ . As shown in Fig. 3, the node-based smoothing domain for node  $k$  is created sequentially connecting the mid-edge-point to the centroids of surrounding  $n$ -sided polygonal elements of node  $k$ ,  $\Gamma_k$  is the boundary of the smoothing domain  $\Omega_k$ . As a result, the number of the smoothing domain is exactly the same as the number of nodes. Each  $n$ -sided polygonal element will be divided into  $n$  quadrilateral sub-domains and each sub-domain is attached to the nearest field node. After obtaining the above-mentioned smoothing domains, the node-based smoothing techniques are applied over these smoothing domains to create a continuous strain field for the NS-FEM model. Then the global smoothed

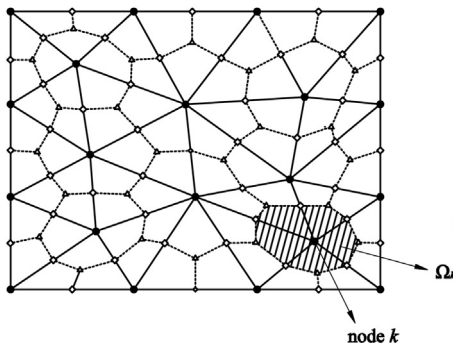


**Fig. 3.** The node-based smoothing domains in 2D problem are created by sequentially connecting the mid-edge-point to the centroids of surrounding  $n$ -sided polygonal elements.

acoustic stiffness matrix of NS-FEM can be obtained as:

$$\bar{\mathbf{K}}^{\text{NS-FEM}} = \int_{\Omega} (\nabla \mathbf{N})^T (\nabla \mathbf{N}) d\Omega = \sum_{k=1}^{N_n} \bar{\mathbf{K}}^{(k)} \quad (30)$$

where  $\mathbf{N}$  denotes the FEM shape functions and  $\bar{\mathbf{K}}^{(k)}$  is the smoothed element stiffness matrix for node  $k$ .

The relation of the acoustic particle velocity  $v$  and the acoustic pressure  $p$  in ideal fluid can be expressed as:

$$\nabla p + j\rho\omega v = 0 \quad (31)$$

where  $j = \sqrt{-1}$ ,  $\rho$  is the density of medium and  $\omega$  is the angular frequency.

In this present formulation, the acoustic particle velocity field  $v$ , which is usually linked to the gradient of acoustic pressure, was smoothed by the node-based smoothing technique and then the smoothed velocity field can be obtained as:

$$\bar{v}(\mathbf{x}_k) = \int_{\Omega_k} v(\mathbf{x}_k) \phi_k(\mathbf{x}) d\Omega \quad (32)$$

where  $\phi_k(\mathbf{x})$  is a given smoothing function that satisfies at least unity property.

$$\int_{\Omega_k} \phi_k(\mathbf{x}) d\Omega = 1 \quad (33)$$

Using the following constant smoothing function

$$\phi_k(\mathbf{x}) = \begin{cases} 1/A_k & x \in \Omega_k \\ 0 & x \notin \Omega_k \end{cases} \quad (34)$$

where  $A_k$  is the area of the smoothing domain for node  $k$ .

Substituting (Eqs. (31) and 34) into Eq. (32) and using Green's theorem, the smoothed velocity field can be obtained in terms of acoustic pressure.

$$\bar{v}(\mathbf{x}_k) = \frac{1}{A_k} \int_{\Omega_k} v(\mathbf{x}) \phi_k(\mathbf{x}) d\Omega = -\frac{1}{j\rho\omega A_k} \int_{\Omega_k} \nabla p d\Omega = -\frac{1}{j\rho\omega A_k} \int_{\Gamma_k} p \cdot \mathbf{n} d\Gamma \quad (35)$$

Using the FEM shape functions, the smoothed velocity field can be expressed in the following matrix form:

$$\bar{v}(\mathbf{x}_k) = -\frac{1}{j\rho\omega} \sum_{i \in M_k} \bar{\mathbf{B}}_i(x_k) p_i \quad (36)$$

where  $M_k$  is total number of nodes in the influence domain of node  $k$ .

$$\bar{\mathbf{B}}_i^T(x_k) = [\bar{b}_{i1} \quad \bar{b}_{i2}] \quad (37)$$

$$\bar{b}_{ip} = \frac{1}{A_k} \int_{\Gamma_k} N_i(x) n_p(x) d\Gamma \quad (38)$$

where  $n_p$  is the outward normal vector on the boundary  $\Gamma_k$ .

Using Gauss integration scheme along the boundary  $\Gamma_k$  of the smoothing domain  $\Omega_k$ , the numerical integration in Eq. (38) can be calculated as

$$\bar{b}_{ip} = \frac{1}{A_k} \sum_{q=1}^{N_s} \sum_{r=1}^{N_g} w_r N_i(x_{qr}) n_p(x_q) \quad (39)$$

where  $N_s$  is the number of segments of the boundary  $\Gamma_k$ ,  $N_g$  is the number Gauss points distributed in each segment and  $w_r$  is the corresponding weight coefficients for Gauss point.

Then the smoothed element stiffness matrix for smoothing domain  $\Omega_k$  in Eq. (30) can be obtained as:

$$\bar{\mathbf{K}}^{(k)} = \int_{\Omega_k} \mathbf{B}^T \mathbf{B} d\Omega = \mathbf{B}^T \mathbf{B} A_k \quad (40)$$

#### 4.2. The hybrid smoothed finite element method for acoustic problems

As mentioned in the published literature (Li et al., 2015), the HS-FEM combines The NS-FEM and the standard FEM by introducing a scaled factor  $\alpha \in [0, 1]$ . In this paper, the problem domain is discretized into three-node triangular elements and the linear FEM shape functions are used. As presented in previous section, in the NS-FEM model each triangular elements in the problems domain will be divided into three quadrilateral sub-domains of equal area by connecting the centroids and mid-edge-point of the triangular elements and each sub-domain contributes to the element stiffness matrix of the node attached. While in the HS-FEM model, as shown in Fig. 4, the difference is that the three original quadrilateral sub-domains at the corners are scaled down by  $(1-\alpha^2)$  with the help of a parameter  $\alpha$ . As a result, the three quadrilateral sub-domains associated with three vertexes have an equal area of  $(1-\alpha^2)A_e/3$  and the remaining Y-shaped sub-domain in the middle of the element has an area of  $\alpha^2 A_e$ , where  $A_e$  is the area of the triangular element.

Then the NS-FEM scheme is used to calculate the contributions to the element stiffness matrix of the three quadrilateral sub-domains and the standard FEM is used to calculate the contributions to the element stiffness matrix of the Y-shaped sub-domain. The global stiffness matrix in HS-FEM can be expressed as:

$$\bar{\mathbf{K}}^{\text{HS-FEM}} = \sum_{k=1}^{N_n} \bar{\mathbf{K}}_k^{\text{NS-FEM}} + \sum_{i=1}^{N_e} \bar{\mathbf{K}}_i^{\text{FEM}} \quad (41)$$

where

$$\bar{\mathbf{K}}_k^{\text{NS-FEM}} = \int_{\Omega_{k,\alpha}^s} (\bar{\mathbf{B}}^\alpha)^T \bar{\mathbf{B}}^\alpha d\Omega \quad (42)$$

$$\bar{\mathbf{K}}_i^{\text{FEM}} = \int_{\Omega_{k,\alpha}^e} \mathbf{B}^T \mathbf{B} d\Omega = \mathbf{B}^T \mathbf{B} \alpha^2 A_i^e \quad (43)$$

where  $\Omega_{k,\alpha}^s$  is the smoothing domain consist of three quadrilateral sub-domains and bounded by  $\Gamma_{k,\alpha}^s$ , as shown in Fig. 5.  $\Omega_{k,\alpha}^e$  is the remaining Y-shaped sub-domain in the original triangular element.

Actually, the smoothed gradient field in the smoothing domain can be calculated as:

$$\bar{\mathbf{B}}^\alpha(\mathbf{x}_k) = \frac{1}{A_{k,\alpha}} \sum_{j=1}^{n_k^e} \frac{1}{3} (1-\alpha^2) A_j^e, \quad \mathbf{B}(\mathbf{x}_k) = \frac{1}{A_k^s} \sum_{j=1}^{n_k^e} \frac{1}{3} A_j^e \mathbf{B}(\mathbf{x}_k) = \bar{\mathbf{B}}(\mathbf{x}_k) \quad (44)$$

where  $A_{k,\alpha}$  is the area of the domain  $\Omega_{k,\alpha}^s$  and  $A_k^s$  is the area defined in Eq. (40),  $n_k^e$  is the number of elements around node  $k$  and  $A_j^e$  is the whole area of the  $j$ th element around node  $k$ .

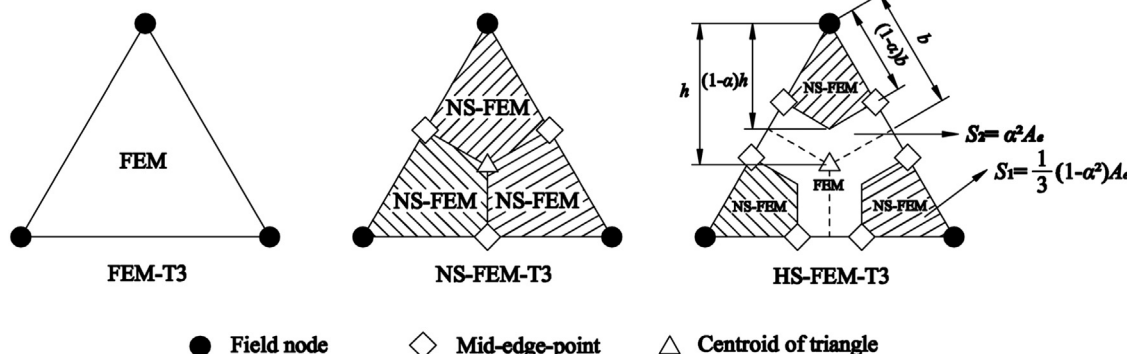


**Fig. 4.** The HS-FEM-T3 elements are formulated by combining FEM-T3 elements and NS-FEM-T3 elements: the NS-FEM is used for three quadrilateral smoothing domains and FEM is used for the remaining Y-shaped area.

Eq. (44) implies that  $\bar{\mathbf{B}}^\alpha$  Eq. (42) can be replaced by  $\bar{\mathbf{B}}(\mathbf{x}_k)$  in Eq. (37), and then Eq. (42) can be rewritten as

$$\bar{\mathbf{K}}_k^{\text{NS-FEM}} = (1-\alpha^2) \bar{\mathbf{B}}^T \bar{\mathbf{B}} A_k^s \quad (45)$$

(Eqs. (43) and 45) show that the procedure of the HS-FEM is very simple and can be implemented in a straightforward way with little change to the original NS-FEM and FEM codes.

#### 5. Dispersion error analysis of acoustic problems using hybrid smoothed finite element method

In this section, the analysis of dispersion error for the HS-FEM is discussed. As shown in Fig. 6, the uniform triangular mesh with constant node spacing of  $h$  is used here and the circles are the nodes contributed to node  $S_{(i,j)}$ . In the standard FEM formulation of 2D acoustic problems, the following set of linear equations can be obtained by assembling the local equations and multiplying the whole set by mesh size  $h$  (He et al., 2010a, 2011a).

$$\begin{aligned} L^{\text{FEM}} = & A_1 p_{ij+1} + A_2 p_{i+1,j+1} + A_1 p_{i-1,j} + A_0 p_{ij} + A_1 p_{i+1,j} \\ & + A_2 p_{i-1,j-1} + A_1 p_{ij-1} = 0 \end{aligned} \quad (46)$$

in which  $L^{\text{FEM}}$  is a row of equation associated with node  $S_{(i,j)}$  in the FEM.

and

$$A_0 = 4 - \frac{1}{2} k^2 h^2 \quad A_1 = -1 - \frac{1}{12} k^2 h^2 \quad A_2 = -\frac{1}{12} k^2 h^2 \quad (47)$$

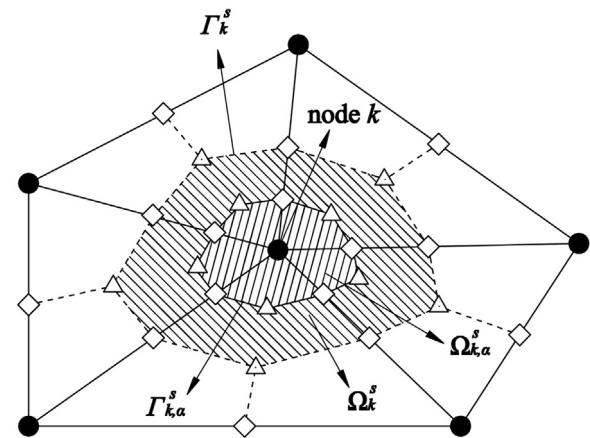


**Fig. 5.** Node-based smoothing domain associated with nodes in the HS-FEM model.

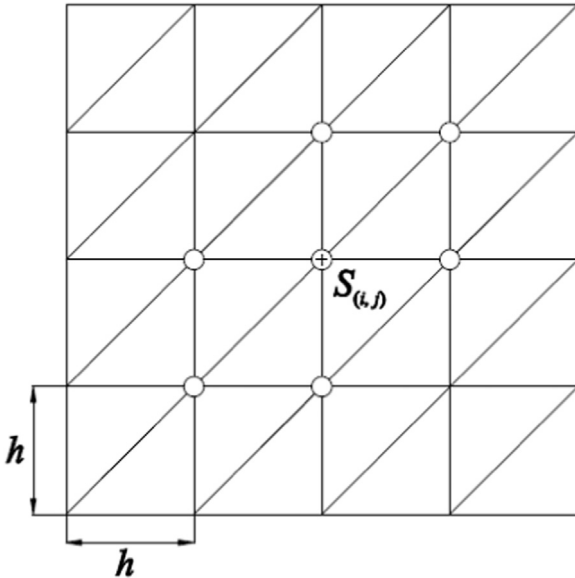


Fig. 6. The uniform triangular mesh with constant node spacing of  $h$ .

For 2D acoustic problems, the expression of a plane wave can be written in the following form

$$p(x) = Ae^{i(k_1 x + k_2 y)} \quad k_1 = k^{\text{FEM}} \cos \theta \quad k_2 = k^{\text{FEM}} \sin \theta \quad (48)$$

in which  $k^{\text{FEM}}$  is the wave number from FEM and  $\theta$  is the wave propagation angle in 2D problems.

Substituting Eq. (48) into (46), Eq. (46) can be written as

$$\begin{aligned} L^{\text{FEM}} = & A_1 e^{i(k_2 h)} + A_2 e^{i(k_1 h + k_2 h)} + A_1 e^{i(-k_1 h)} + A_0 + A_1 e^{i(k_1 h)} \\ & + A_2 e^{i(-k_1 h - k_2 h)} + A_1 e^{i(-k_2 h)} = 0 \end{aligned} \quad (49)$$

Then the following equation can be obtained easily

$$\text{Re}(L^{\text{FEM}}) = A_0 + 2A_1(\cos(k_1 h) + \cos(k_2 h)) + 2A_1 \cos(k_1 h + k_2 h) = 0 \quad (50)$$

By substituting (Eqs. (47) and 48) into Eq. (50), the relation between the exact wave number  $k$  and  $k^{\text{FEM}}$  from FEM can be obtained as

$$k^2 = \frac{1}{h^2} \frac{24 - 12(\cos(k_1 h) + \cos(k_2 h))}{3 + (\cos(k_1 h) + \cos(k_2 h) + \cos(k_1 h + k_2 h))} \quad (51)$$

Using the Taylor series expansion of  $k$  in the terms of  $k^{\text{FEM}}$  and performing some simplifications, the above equation becomes

$$k = k^{\text{FEM}} + \frac{(k^{\text{FEM}})^3 h^2}{24} \left( \frac{1}{2} \sin^2 2\theta + \sin 2\theta + 1 \right) + O((k^{\text{FEM}})^5) \quad (52)$$

Eq. (52) can also be expressed as following

$$k^{\text{FEM}} = k - \frac{(k^{\text{FEM}})^3 h^2}{24} \left( \frac{1}{2} \sin^2 2\theta + \sin 2\theta + 1 \right) + O((k^{\text{FEM}})^5) \quad (53)$$

In the right hand of Eq. (53),  $k^{\text{FEM}} \approx k$  is valid and Eq. (53) can be rewritten as

$$k^{\text{FEM}} = k - \frac{k^3 h^2}{24} \left( \frac{1}{2} \sin^2 2\theta + \sin 2\theta + 1 \right) + O(k^5) \quad (54)$$

From Eq. (54), it is clear that the dispersion error of FEM can be expressed as

$$e^{\text{FEM}} = \left| \frac{k^2 h^2}{24} \left( \frac{1}{2} \sin^2 2\theta + \sin 2\theta + 1 \right) + O(k^4) \right| \quad (55)$$

Following the similar steps, the wave number  $k^{\text{NS-FEM}}$  from NS-FEM in 2D acoustic problems can be obtained (He et al., 2010a, 2015):

$$k^{\text{NS-FEM}} = k + \frac{k^3 h^2}{24} (\sin 2\theta + 2) + O(k^5) \quad (56)$$

The dispersion error of NS-FEM can be expressed as

$$e^{\text{NS-FEM}} = \left| \frac{k^2 h^2}{24} (\sin 2\theta + 2) + O(k^4) \right| \quad (57)$$

From (Eqs. (54) and 56), it is clear that the wave number  $k^{\text{FEM}}$  obtained from FEM is always smaller than the exact one and the wave number  $k^{\text{NS-FEM}}$  obtained from NS-FEM is always larger than the exact one. This interesting phenomenon may result from the “overly-stiff” property of the FEM and the “overly-soft” property of the NS-FEM. Therefore, it may be reasonable to combine with the FEM and NS-FEM to obtain a “close-to-exact” stiffness of the discretized model with the help of a parameter  $\alpha \in [0, 1]$ . By carefully choosing the value of parameter  $\alpha$  which controls the contributions from both FEM and NS-FEM, it may be possible to relieve or eliminate the dispersion error in acoustic problems.

He et al. (2015) showed that the wave number  $k^{\text{HS-FEM}}$  from HS-FEM can be derived and expressed as follows

$$k^{\text{HS-FEM}} = k - \frac{k^3 h^2}{24} \left( \frac{1}{2} (1 - \alpha^2) \sin^2 2\theta + (1 - 2\alpha^2) \sin 2\theta + 1 - 3\alpha^2 \right) + O(k^5) \quad (58)$$

And the dispersion error of HS-FEM becomes

$$e^{\text{HS-FEM}} = \left| \frac{k^2 h^2}{24} \left( \frac{1}{2} (1 - \alpha^2) \sin^2 2\theta + (1 - 2\alpha^2) \sin 2\theta + 1 - 3\alpha^2 \right) + O(k^4) \right| \quad (59)$$

From Eqs. (53), (56) and (58), it is obvious that the HS-FEM is exactly the same with NS-FEM when  $\alpha=1$  and if  $\alpha=0$ , HS-FEM will become standard FEM. In addition, it also can be seen from (Eqs. (58) and 59) that the dispersion error of HS-FEM not only depends on the wave number  $k$  and wave propagation angle  $\theta$  but also depends on the parameter  $\alpha$ . Therefore, the determination of the value of  $\alpha$  is a crucial issue in the analysis of acoustic problems using HS-FEM.

In fact, it is quite difficult to determine the optimal value of  $\alpha$ . However, if  $\alpha^2=0.5$ , Eq. (59) can be expressed as

$$\left| \frac{1}{4} \frac{k^2 h^2}{24} + O(k^4) \right| \leq \underbrace{\left| \frac{k^2 h^2}{24} \left( \frac{1}{4} \sin^2 2\theta - \frac{1}{2} \right) + O(k^4) \right|}_{e^{\text{HS-FEM}}} \leq \left| \frac{1}{2} \frac{k^2 h^2}{24} + O(k^4) \right| \quad (60)$$

More importantly, the following equations can be obtained from (Eqs. (53) and 57) easily for arbitrary wave number  $k$  and wave propagation angle  $\theta$ .

$$\left| \frac{1}{2} \frac{k^2 h^2}{24} + O(k^4) \right| \leq \underbrace{\left| \frac{k^2 h^2}{24} \left( \frac{1}{2} \sin^2 2\theta + \sin 2\theta + 1 \right) + O(k^4) \right|}_{e^{\text{FEM}}} \leq \left| \frac{5}{2} \frac{k^2 h^2}{24} + O(k^4) \right| \quad (61)$$

$$\left| \frac{k^2 h^2}{24} + O(k^4) \right| \leq \underbrace{\left| \frac{k^2 h^2}{24} (\sin 2\theta + 2) + O(k^4) \right|}_{e^{\text{NS-FEM}}} \leq \left| 3 \cdot \frac{k^2 h^2}{24} + O(k^4) \right| \quad (62)$$

From (Eqs. (60)–62), it is clear that if  $\alpha^2=0.5$  is adopted; HS-FEM will always behave better than FEM and NS-FEM. This  $\alpha$  may not be optimal and the solution also may not be very close to the exact one, but the accuracy of HS-FEM is still better than FEM and

NS-FEM. Therefore,  $\alpha^2=0.5$  is adopted for all the numerical examples in this paper.

## 6. Numerical error for acoustic problems

It is well known that the quality of the numerical solution for acoustic problems using FEM depends on wave numbers  $k$  as well as the average mesh size  $h$  of the numerical model. For practical applications, acoustic finite element users usually follow the so-called “the rule of thumb” to obtain acceptable solution. According to “the rule of thumb”, a wave-length should always be resolved by a constant number of elements. However, this rule can only provide reliable results in the low frequency range. For high frequency range, it cannot work well and the numerical error may be prohibitive.

As the published literature mentioned (Ihlenburg et al., 1997), the numerical error indicator in the  $H^1$ -semi-norm can be expressed as:

$$e_n^2 = |p^e - p^h|^2 = \int_{\Omega} (\tilde{v}^e - \tilde{v}^h)^T (v^e - v^h) d\Omega \quad (63)$$

where  $\tilde{v}$  is the complex conjugate of the velocity, the superscript  $e$  denotes the exact solutions and  $h$  denotes the numerical solutions obtained from numerical methods including the present HS-FEM and standard FEM.

Ihlenburg et al. (1997) proved that the relative error of the  $hp$ -version FEM solution for acoustic problem in  $H^1$ -semi-norm is bounded by

$$\eta = \frac{|p^e - p^h|}{|p^e|} = \sqrt{\frac{\int_{\Omega} (\tilde{v}^e - \tilde{v}^h)^T (v^e - v^h) d\Omega}{\int_{\Omega} (\tilde{v}^e \cdot v^e)^2 d\Omega}} \leq C_1 \left(\frac{kh}{p}\right)^p + C_2 k \left(\frac{kh}{p}\right)^{2p} \quad (64)$$

where  $p$  is the degree of polynomial approximation used in the numerical methods.

Ihlenburg et al. (1997) proved that the numerical error can be split into two terms: the first term in Eq. (64) denotes the interpolation error. This error can be controlled by keeping  $kh$  constant. The second term denotes the numerical pollution error caused not only by phase shift but also the error on the amplitude of the wave.

For linear interpolation ( $p=1$ ) discussed in this paper, the pollution error term can be neglected if  $kh < 1$ , so the relative error is mainly caused by the interpolation error term for small wave numbers. While for large wave numbers, the pollution error term will dominates the relative error, because it will increase linearly with the increase of wave number  $k$ .

In this present paper, the relative error of the numerical solution obtained from the standard FEM and HS-FEM will be discussed in details. The numerical results demonstrate that the numerical error will reduce significantly due to the gradient smoothing operation on the numerical model and the HS-FEM can obtain more accurate results than the standard FEM.

## 7. Numerical results

In this section, a number of numerical results are presented to test the efficiency and accuracy of the methods we have proposed. For acoustic problems, we have known that the wave number solution of FEM is always smaller than the exact solution due to the “overly-stiff” property of the model and the NS-FEM solution is always larger than the exact one due to the “overly-soft” property, so it is possible to combine with the FEM and NS-FEM to obtain a proper stiffness of the model for reducing dispersion error. As

indicated in (Eqs. (60)–62), when  $\alpha^2=0.5$ , HS-FEM will always behave better than FEM and NS-FEM.

### 7.1. Circular scatter

The first benchmark problem considered is the scattering from a single rigid cylinder with infinite length located in the unbounded domain. As shown in Fig. 7, the direction of the incident plane wave is along  $x$ -axis. The density of the medium is  $1000 \text{ kg/m}^3$  and the speed of the wave is  $1500 \text{ m/s}$ . This problem can be simplified as a general two-dimensional acoustic scattering problem even if it is a three dimensional problem since the geometry of the problem domain is prismatic. The circular obstacle with radius  $a=0.2$  is located at  $(0, 0)$ . The artificial boundary  $B$  with the center at  $(0, 0)$  is a circle with radius  $R=1$ . The analytical solution of far-field pattern for this scattering problem can be easily derived and the scattered acoustic pressure field are given by:

$$p = \sum_{n=0}^{\infty} \left[ -(-j)^n \epsilon_n \frac{\frac{d}{dk} J_n(ka)}{\frac{d}{dk} H_n^{(2)}(ka)} \right] H_n^{(2)}(kr) \cos(n\theta) \quad (65)$$

where  $k$  is the wave number,  $J_n(x)$  denotes the Bessel function of the first kind,  $H_n(x)$  denotes the Hankel function of the second kind.  $\theta$  is the scattering angle. In Eq. (65), when  $n=0$ ,  $\epsilon_n=1$ , otherwise  $\epsilon_n=2$ .

#### 7.1.1. Accuracy of the scattered acoustic field

In order to test the performance of the proposed method, three different wave numbers ( $k=2\pi, k=5\pi$  and  $k=8\pi$ ) have been employed to study this acoustic scattering problem using HS-FEM with average mesh size of 0.04. Figs. 8 and 9 show the scattering patterns of total pressure and the numerical error at different wave numbers for the circular scatter, respectively. For the purpose of comparison, the analytical solutions and the numerical results from the standard FEM and GLS (Harari and Nogueira, 2002) using the same mesh are also presented in the figures. It can be seen from the figures that both FEM, GLS and HS-FEM can provide reliable results which agree well with the exact solution at small wave number, while at large wave number, the numerical results obtained from FEM may depart from the exact solution, the results of HS-FEM are still in good agreement with the exact one and even behaves better than GLS using triangular elements which has been proved to be a very effective approach to reduce dispersion error for acoustic problems. This numerical example demonstrates that HS-FEM can provide very properly softened stiffness of the numerical model and can achieve more accurate results than the FEM and GLS, especially for large wave numbers.

More details, the scattered acoustic pressure on the artificial boundary as a function of the wave number at two critical points with two polar angles ( $\theta=0$  and  $\theta=\pi/4$ ) are also considered. In order to study the numerical results clearly, the real part and

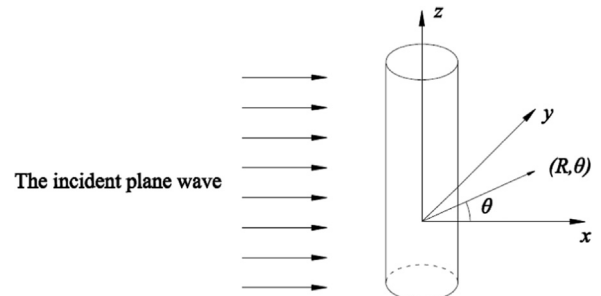
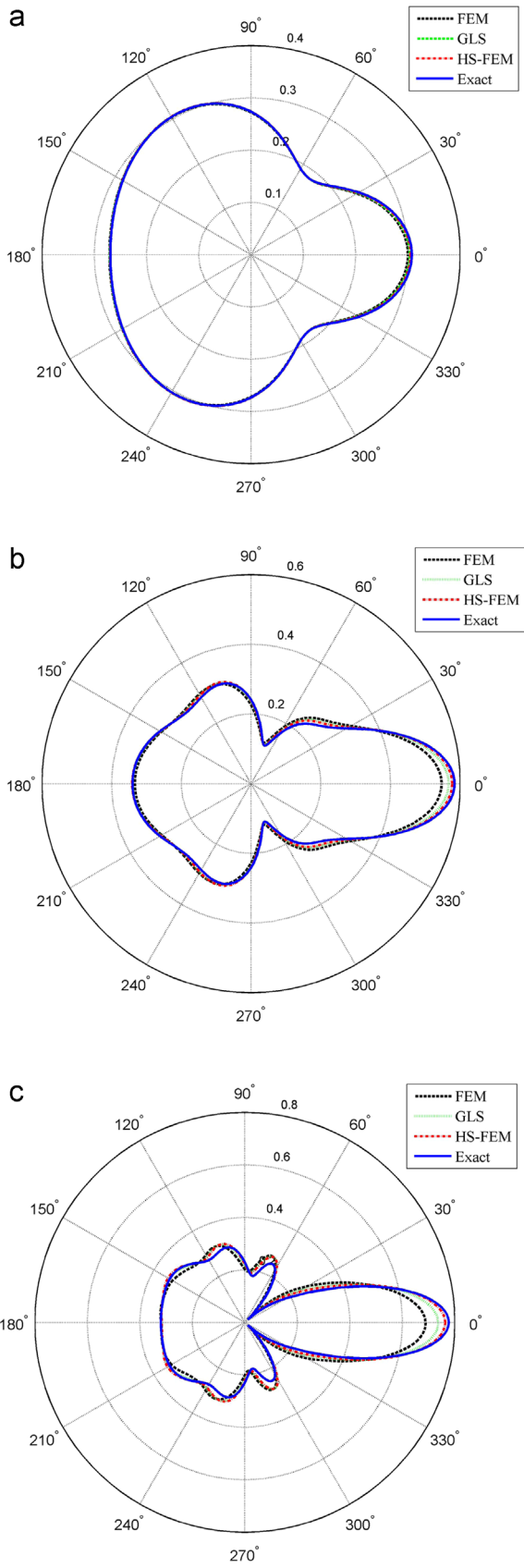
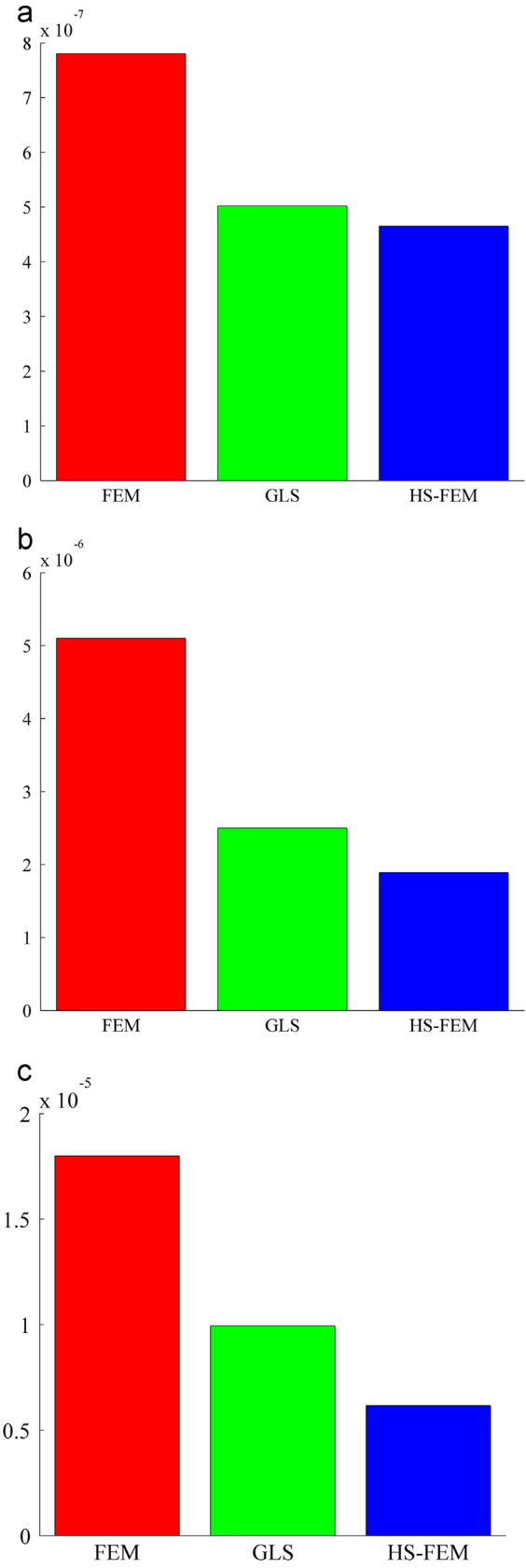


Fig. 7. The acoustic scattering from a single rigid cylinder with infinite length located in the unbounded domain.



**Fig. 8.** The scattering pattern at different wave numbers on the artificial boundary for the rigid circular cylinder: (a)  $k = 2\pi$ ; (b)  $k = 5\pi$ ; (c)  $k = 8\pi$ .



**Fig. 9.** The numerical error at different wave numbers for the rigid circular cylinder: (a)  $k = 2\pi$ ; (b)  $k = 5\pi$ ; (c)  $k = 8\pi$ .

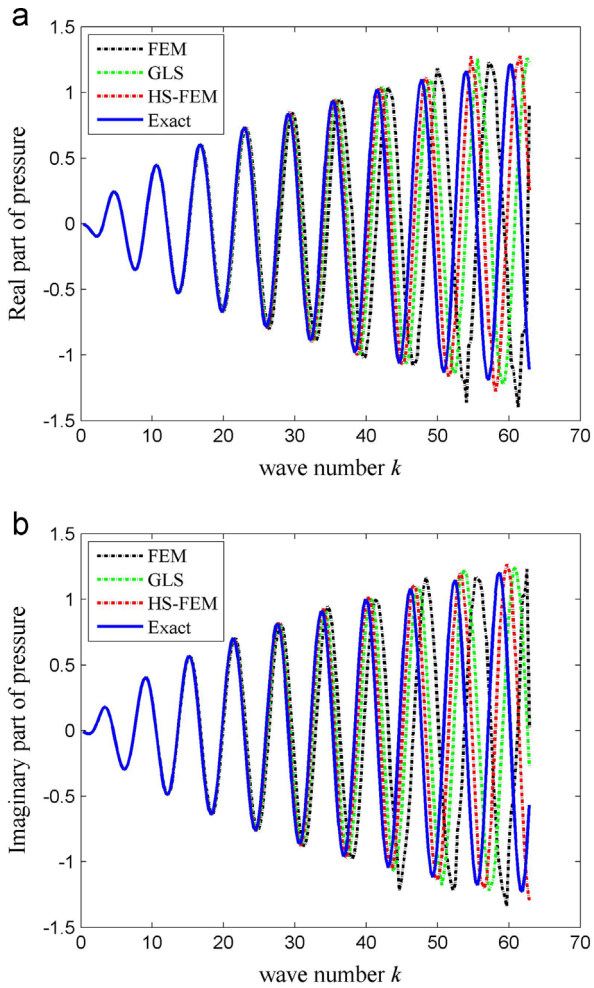


**Fig. 10.** The scattered acoustic pressure on the artificial boundary as a function of the wave number at the point with polar angle  $\theta=0$ : (a) The real part of the pressure. (b) The imaginary part of the pressure.

imaginary part of pressure are plotted separately. The HS-FEM, GLS, FEM and exact results are depicted in Figs. 10 and 11. From the results, it can be seen that both HS-FEM, GLS and FEM results agree fairly well the exact solution for small wave number. With the increase of wave number, the accuracy of all the results obtained using the numerical method will deteriorate and depart from the exact solutions. While compared to FEM, the present HS-FEM can provide more accurate results, more importantly, the present HS-FEM are even a little better than GLS. This again verifies the efficiency of the present HS-FEM for solving acoustic scattering problems.

#### 7.1.2. Convergence study

This section will investigate the convergence rate of the present HS-FEM for scattering acoustic problems by employing several different meshes. Fig. 12 depicts the relative error as a function of the average mesh size at different wave numbers of  $k=3\pi$  and  $k=6\pi$  for both HS-FEM and FEM results. For the purpose of giving a comparison, the numerical results from GLS are also plotted in the figure. It can be found from the figure that: for small wave number ( $k=3\pi$ ), the relative error of both HS-FEM and FEM are about 10%, while the results of present HS-FEM are more accurate than that of FEM results and even surpass GLS results. Besides, the results of HS-FEM converge faster than that of FEM and GLS do when the mesh gets finer. For large wave number ( $k=6\pi$ ), the relative error of both HS-FEM and FEM will increase significantly,

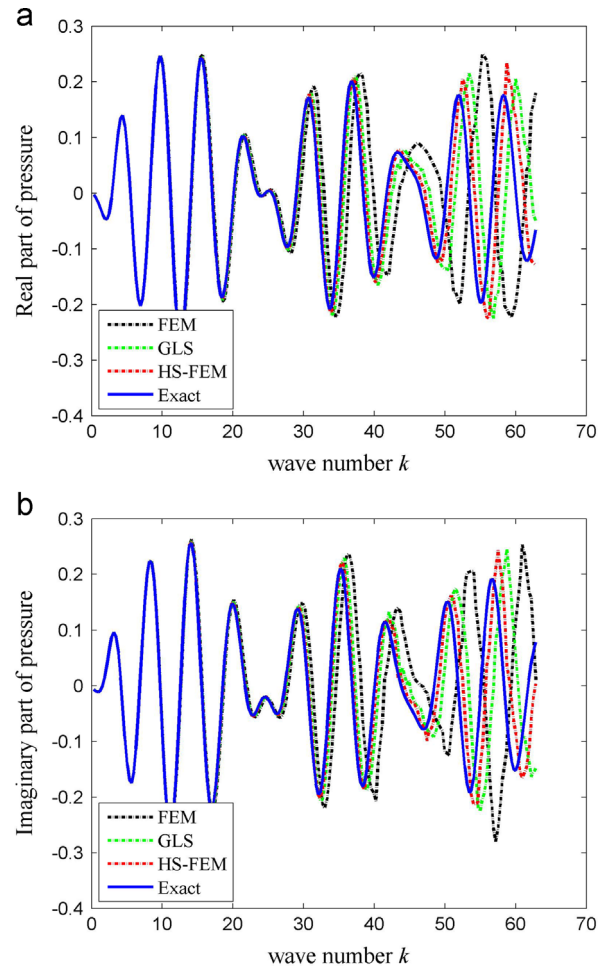


**Fig. 11.** The scattered acoustic pressure on the artificial boundary as a function of the wave number at the point with polar angle  $\theta=\pi/4$ : (a) The real part of the pressure. (b) The imaginary part of the pressure.

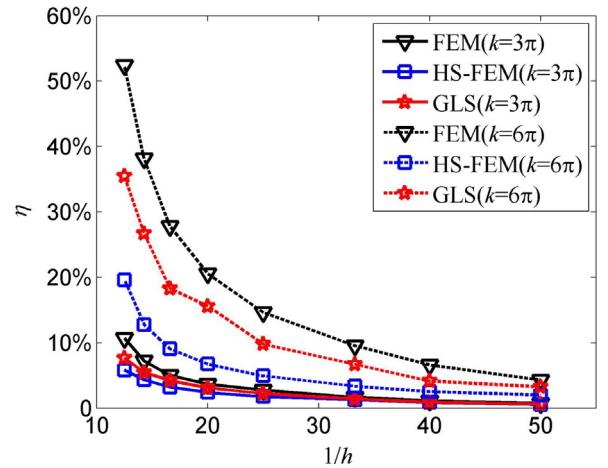


**Fig. 12.** Comparison of convergence rate of the results from HS-FEM and FEM with different meshes.

compared to FEM and GLS, the HS-FEM solutions are obviously better. These findings show that HS-FEM works very well and converges much faster than FEM and GLS.

#### 7.1.3. Control of the numerical error

Eq. (64) shows the upper bound of the relative error in  $H^1$  semi-norm for the method of  $hp$  version. For linear elements ( $p=1$ ) used

in this paper, the relative error is bounded by:

$$\eta = \frac{\|p^e - p^h\|_1}{\|p^e\|_1} = \sqrt{\frac{\int_{\Omega} (\tilde{v}^e - \tilde{v}^h)^T (v^e - v^h) d\Omega}{\int_{\Omega} (\tilde{v}^e \cdot v^e)^2 d\Omega}} \leq C_1 kh + C_2 k^3 h^2 \quad (66)$$

**Eq. (66)** means that the control of the relative error requires considering both  $kh$  and  $k^3 h^2$ . **Fig. 13** shows the relative error against the wave number  $k$  for both HS-FEM, GLS and FEM solutions.

For the purpose of discuss, cases of  $kh=1$  (the interpolation error) and  $k^3 h^2=1$  (the pollution error) are also plotted in the figure. It can be observed from the figure that the relative error obtained from HS-FEM, GLS and FEM are both very small for low wave numbers. However, the relative errors increase quickly as the wave number  $k$  grows, while HS-FEM performs better than the FEM and GLS, and can achieve more accurate results for the full wave number range.

Furthermore, in order to study the control of numerical error with the present method clearly. The relative errors are computed on a range of different meshes by keeping  $kh = \text{cst}$  and  $k^3 h^2 = \text{cst}$ . **Fig. 14** shows the relative error against  $1/h$  with varying  $h$  and keeping  $kh$  constant using HS-FEM, GLS and FEM. From the results in **Fig. 14**, it can be found that: for small wave number range, the interpolation error (the first term in **Eq. (66)**) is well controlled if  $kh$  is kept constant for both HS-FEM, GLS and FEM; for large wave number range, the upper bound of the relative error of FEM results will increase dramatically, while the HS-FEM and GLS results are better than FEM. In addition, the HS-FEM even behaves a little better than GLS for the total wave number range. It means that the pollution error will dominate the relative error because the pollution error (the second term in **Eq. (66)**) will increase linearly with wave number  $k=1/h$ . While the HS-FEM results do not deteriorate significantly with the increase of  $k$ . This means that a certain level of relative error can be controlled by the gradient smoothing techniques used in the HS-FEM. **Fig. 15** shows the relative error against  $1/h$  with varying  $h$  and keeping  $k^3 h^2$  constant. From the results in **Fig. 15**, the upper bound of relative error is well controlled for both HS-FEM, GLS and FEM if  $k^3 h^2$  is kept constant. This is because not only the interpolation error but also the pollution error can be controlled in the case  $k^3 h^2 = \text{cst}$  based on **Eq. (66)**. Compared to FEM and GLS, the HS-FEM still provide more stable results.

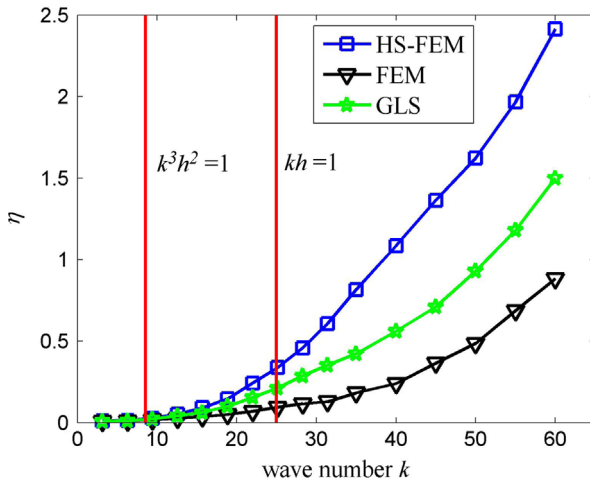


**Fig. 13.** The relative error in the  $H^1$  semi-norm against the wave number  $k$  for both HS-FEM and FEM solutions.

## 7.2. Elliptical scatter

In this example, a benchmark problem of a rigid elliptical scatter is investigated to again check and verify the property of the proposed HS-FEM. As shown in **Fig. 16**, the elliptical scatter with an aspect ratio  $a/b = 2$  ( $a=0.2$  and  $b=0.1$ ) is located at  $(0, 0)$ . The artificial boundary  $B$  is still a circle of radius  $R=1$  with center at  $(0, 0)$ . The incident plane wave and fluid medium are the same as the problem discussed in previous section. The computational domain is discretized into 1480 nodes and 2800 triangular elements.

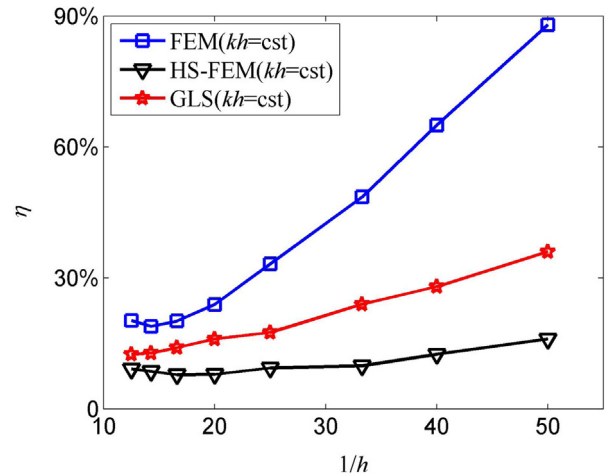


**Fig. 14.** Evolution of the relative error in  $H^1$  semi-norm as a function of  $1/h$  with varying  $h$  and keeping  $kh$  constant.

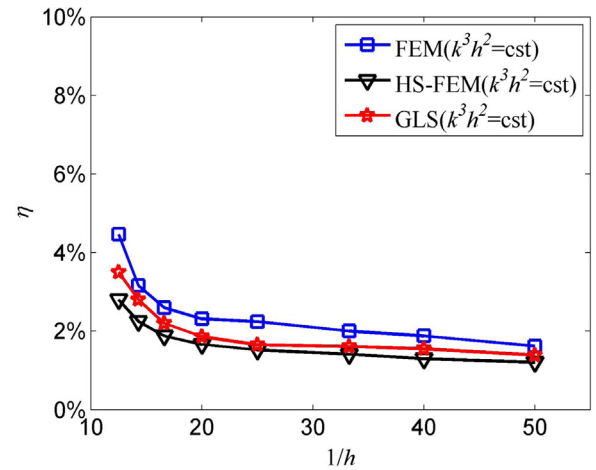


**Fig. 15.** Evolution of the relative error in  $H^1$  semi-norm as a function of  $1/h$  with varying  $h$  and keeping  $k^3 h^2$  constant.

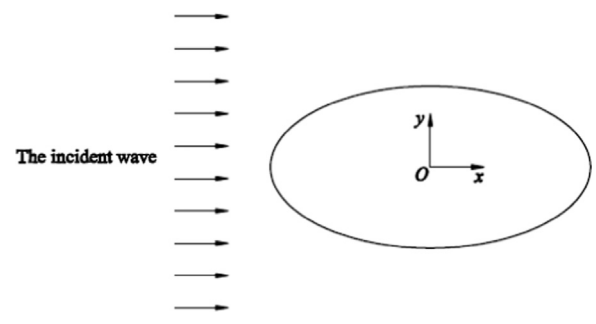


**Fig. 16.** The rigid elliptical scatter.

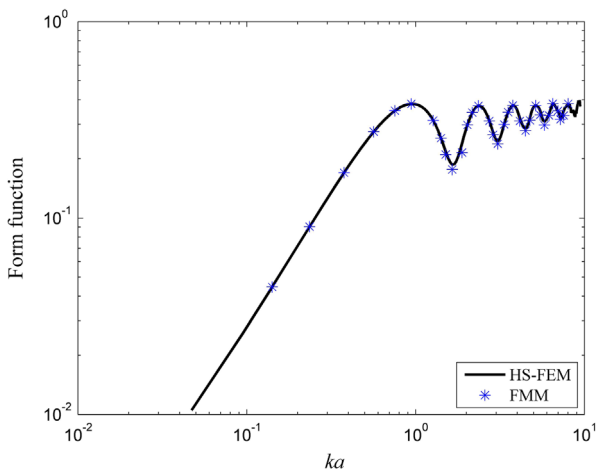


**Fig. 17.** The magnitude of the backscattering form function for the rigid elliptical scatter.

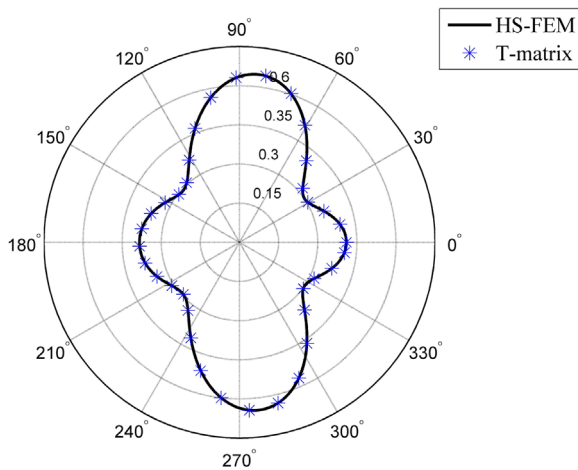


**Fig. 18.** The scattering pattern at non-dimensional wave number  $ka=2$  for the rigid elliptical scatter.

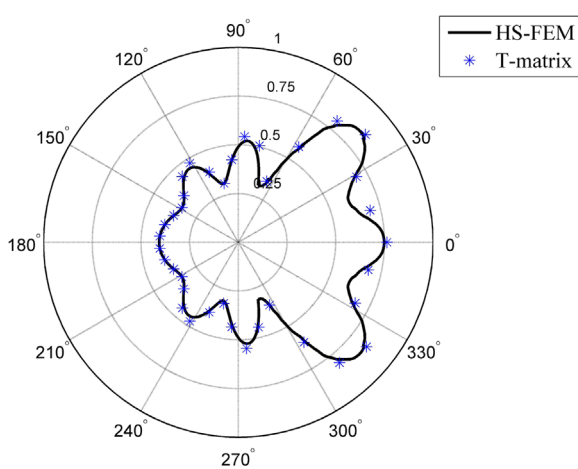


**Fig. 19.** The scattering pattern at non-dimensional wave number  $ka=5$  for the rigid elliptical scatter.

**Fig. 17** shows the magnitude of the backscattering form function for the rigid elliptical scatter. The solid line is computed using HS-FEM presented here, while the stars correspond to the numerical calculations obtained from DiPerna and Standon's

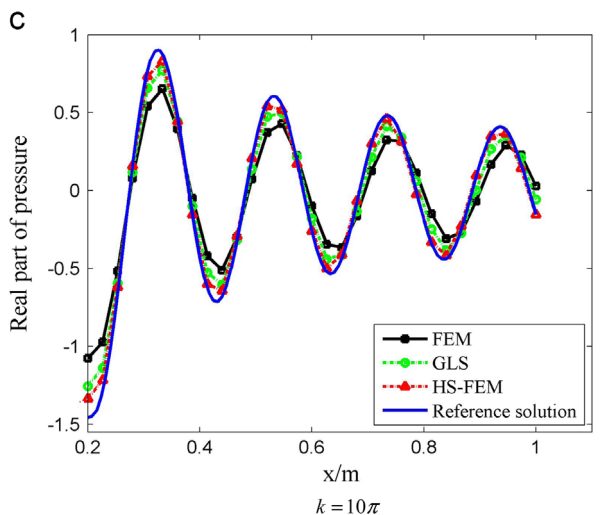
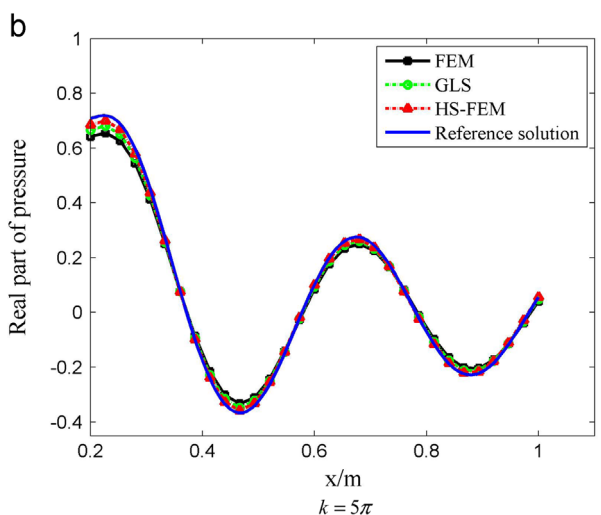
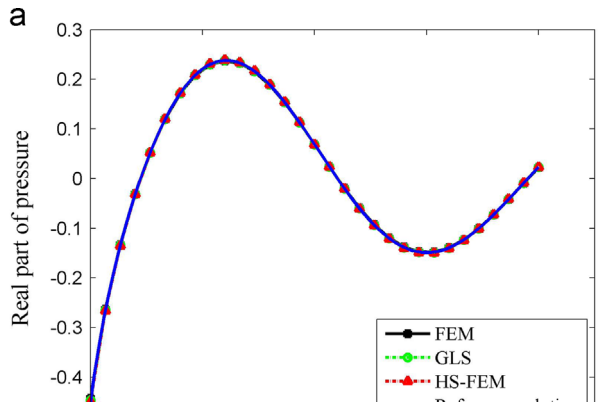


**Fig. 20.** The real part of the acoustic pressure along  $x$ -axis at different wave numbers for the rigid elliptical scatter. (a)  $k = 3\pi$ . (b)  $k = 5\pi$ . (c)  $k = 10\pi$ .

results using Fourier matching method (FMM) (DiPerna and Stanton, 1994). From the figure, it is found that the HS-FEM results are in good agreement with the FMM results and it is demonstrated that HS-FEM is effective and reliable to solve acoustic scattering problems.

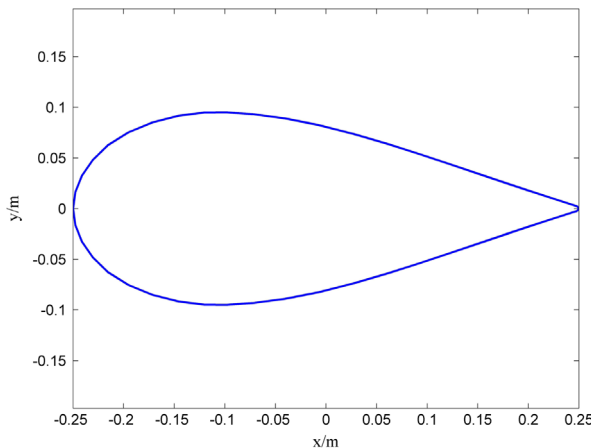


**Fig. 21.** The geometry of the rigid rudder-shaped scatter.

Furthermore, the scattering pattern at different non-dimensional wave numbers ( $ka=2$  and  $ka=5$ ) for the rigid elliptical scatter are also computed to check and verify the results from HS-FEM, as shown in Figs. 18 and 19. The solid lines represent the numerical results obtained from HS-FEM, while the stars represent the numerical results obtained from the well-known  $T$ -matrix method (Pillai et al., 1982). As noticed from the figures, good agreement is found between the results of the two methods. This again verifies that HS-FEM is of effectiveness in solving acoustic scattering problems.

More details, in order to compare and discuss the numerical results obtained from HS-FEM and FEM, the real part of the acoustic pressure along  $x$ -axis at different wave numbers ( $k = 3\pi, k = 5\pi$  and  $k = 10\pi$ ) are plotted in Fig. 20. For the purpose of giving a comparison, the results obtained from GLS with the same mesh and a reference results obtained from FEM with a very fine mesh are also presented in the figures. From these figures, it is found that all the acoustic pressure obtained from HS-FEM, GLS and FEM are very close to the reference results for small wave numbers. When it comes to large wave numbers, the HS-FEM results do not deviate much from the reference results and even behave a little better than GLS, while the corresponding results from FEM depart from the reference results a lot. These findings validate that HS-FEM can provide more accurate solution than FEM and be a good competitor to GLS for acoustic scattering problems, especially for large wave numbers.

### 7.3. Rudder-shaped scatter

This example is concerned with the numerical analysis of the acoustic scattering from a rigid rudder-shaped scatter. The model is described in Fig. 21. The mesh of this model consists of 1557 nodes with 2970 elements and three different wave numbers ( $k = 3\pi, k = 6\pi$  and  $k = 8\pi$ ) are considered here. The boundary conditions and acoustic source are the same as described in previous section. The scattered acoustic pressure distributions of HS-FEM, GLS and FEM along the  $x$ -axis are depicted in Fig. 22. As the exact solution for this problem is not available, the corresponding reference results obtained using FEM with a high quality mesh are also plotted in the figures for comparison. As shown in the figures, all the numerical methods can provide very accurate results for small wave numbers. With the increase of the wave numbers, the FEM results may deteriorate quickly, while the results from HS-FEM and GLS are similar and much closer to the reference results than FEM. From this numerical example, it is again verified that HS-FEM performs better and can give more accurate results than FEM for acoustic scattering problems.

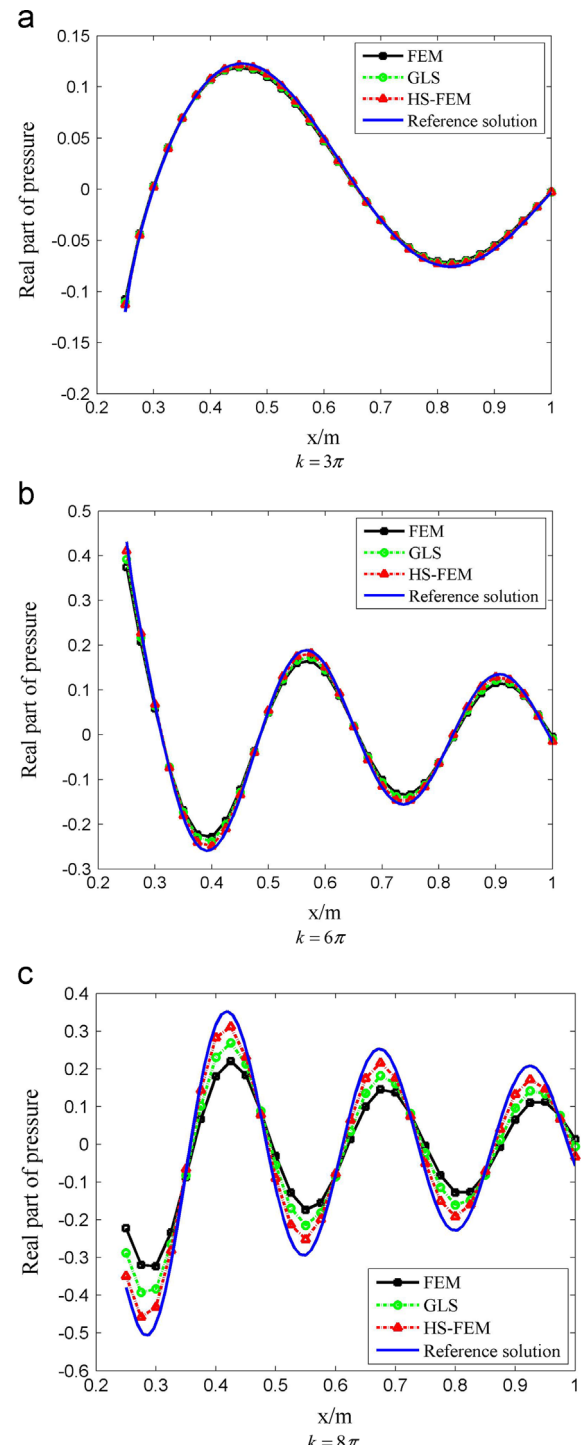


**Fig. 22.** The real part of the acoustic pressure along  $x$ -axis at different wave numbers for the rudder-shaped scatter. (a)  $k = 3\pi$ . (b)  $k = 6\pi$ . (c)  $k = 8\pi$ .

## 8. Conclusions

In this paper, coupling of the hybrid smoothed finite element method (HS-FEM) was combined with the Dirichlet-to-Neumann (DtN) boundary condition to give a HS-FEM-DtN model for two-dimensional underwater acoustic scattering problems. A number of numerical examples are investigated in detail to examine the accuracy, convergence and numerical error control of the present method. The following conclusions can be drawn from the numerical results.

- 1) Coupling of the HS-FEM and the well known DtN boundary condition works well for two-dimensional underwater acoustic scattering problems and can provide very stable numerical results.
- 2) For the two-dimensional underwater acoustic scattering problems discussed in this paper, the HS-FEM program using triangular elements is very simple since no additional parameters or degrees of freedoms are needed and hence it can be implemented directly with little change to the original FEM code.
- 3) Compared with the standard FEM, the present method can provide an appropriately softened effect and close-to-exact stiffness to the model owing to the gradient smoothing operation. Therefore, the HS-FEM can obtain much more accurate results than the FEM does.
- 4) For the practical underwater acoustic scattering problems with complicated geometry, the HS-FEM performs better than the FEM with the same mesh. It indicates that the HS-FEM is capable of solving the real engineering problems with very accurate results.

## Acknowledgments

The authors wish to express their gratitude to the National Natural Science Foundation of China (Contract no. 51379083, 51579109 and 51579112).

## References

- Berenger, J.P., 1994. A perfectly matched layer for the absorption of electromagnetic waves. *J. Comput. Phys.* 114 (2), 185–200.
- Belytschko, T., Lu, Y.Y., Gu, L., 1994. Element-free Galerkin methods. *Int. J. Numer. Methods Eng.* 37 (2), 229–256.
- Boulliard, P., Suleaub, S., 2008. Element-Free Galerkin solutions for Helmholtz problems: formulation and numerical assessment of the pollution effect. *Comput. Meth. Appl. Mech. Eng.* 162 (1), 317–335.
- Clayton, R., Engquist, B., 1977. Absorbing boundary conditions for acoustic and elastic wave equations. *Bull. Seismol. Soc. Am.* 67 (6), 1529–1540.
- Crocker, M.J., 1975. Prediction of transmission loss in mufflers by the finite-element method. *J. Acoust. Soc. Am.* 57 (1), 144–148.
- DiPerna, D.T., Stanton, T.K., 1994. Sound scattering by cylinders of noncircular cross section: a conformal mapping approach. *J. Acoust. Soc. Am.* 96 (5), 3064–3079.
- Deraemaeker, A., Babuška, I., Boulliard, P., 1999. Dispersion and pollution of the FEM solution for the Helmholtz equation in one, two and three dimensions. *Int. J. Numer. Methods Eng.* 46 (4), 471–499.
- Engquist, B., Majda, A., 1977. Absorbing boundary conditions for numerical simulation of waves. *Proc. Natl. Acad. Sci. USA* 74 (5), 1765–1766.
- Franca, L.P., Farhat, C., Maceo, A.P., Lesoinne, M., 1997. Residual-free bubbles for the Helmholtz equation. *Int. J. Numer. Methods Eng.* 40 (21), 4003–4009.
- Grote, M.J., Kirsch, C., 2004. Dirichlet-to-Neumann boundary conditions for multiple scattering problems. *J. Comput. Phys.* 201 (2), 630–650.
- Givoli, D., Patlashenko, I., Keller, J.B., 1998. Discrete Dirichlet-to-Neumann maps for unbounded domains. *Comput. Meth. Appl. Mech. Eng.* 164 (1), 173–185.
- Harari, I., Hughes, T.J.R., 1992. Galerkin/least-squares finite element methods for the reduced wave equation with non-reflecting boundary conditions in unbounded domains. *Comput. Methods Appl. Mech. Eng.* 98 (3), 411–454.
- Harari, I., Magoulès, F., 2004. Numerical investigations of stabilized finite element computations for acoustics. *Wave Motion* 39 (4), 339–349.
- Harari, I., Nogueira, C.L., 2002. Reducing dispersion of linear triangular elements for the Helmholtz equation. *J. Eng. Mech. ASCE* 128 (3), 351–358.
- Harari, I., Patlashenko, I., Givoli, D., 1998. Dirichlet-to-Neumann maps for unbounded wave guides. *J. Comput. Phys.* 143 (1), 200–223.
- Hastings, F.D., Schneider, J.B., Broschat, S.L., 1996. Application of the perfectly matched layer (PML) absorbing boundary condition to elastic wave propagation. *J. Acoust. Soc. Am.* 100 (5), 3061–3069.
- He, Z.C., Li, E., Li, G.Y., Wu, F., Liu, G.R., Nie, X., 2015. Acoustic simulation using  $\alpha$ -FEM with a general approach for reducing dispersion error. *Eng. Anal. Bound. Elem.* 61, 241–253.
- He, Z.C., Liu, G.R., Zhong, Z.H., Wu, S.C., Zhang, G.Y., Cheng, A.G., 2009. An edge-based smoothed finite element method (ES-FEM) for analyzing three-dimensional acoustic problems. *Comput. Meth. Appl. Mech. Eng.* 199 (1), 20–33.
- He, Z.C., Liu, G.R., Zhong, Z.H., Zhang, G.Y., Cheng, A.G., 2010a. Dispersion free analysis of acoustic problems using the alpha finite element method. *Comput. Mech.* 46 (6), 867–881.
- He, Z.C., Liu, G.R., Zhong, Z.H., Cui, X.Y., Zhang, G.Y., Cheng, A.G., 2010b. A coupled edge-/face-based smoothed finite element method for structural-acoustic problems. *Appl. Acoust.* 71 (10), 955–964.
- He, Z.C., Cheng, A.G., Zhang, G.Y., Zhong, Z.H., Liu, G.R., 2011a. Dispersion error reduction for acoustic problems using the edge-based smoothed finite element method (ES-FEM). *Int. J. Numer. Methods Eng.* 86 (11), 1322–1338.
- He, Z.C., Liu, G.R., Zhong, Z.H., Zhang, G.Y., Cheng, A.G., 2011b. A coupled ES-FEM/BEM method for fluid-structure interaction problems. *Eng. Anal. Bound. Elem.* 35 (1), 140–147.
- He, Z.C., Li, G.Y., Zhong, Z.H., Cheng, A.G., Zhang, G.Y., Li, E., Liu, G.R., 2012. An ES-FEM for accurate analysis of 3D mid-frequency acoustics using tetrahedron mesh. *Comput. Struct.* 106, 125–134.
- Higdon, R.L., 1987. Numerical absorbing boundary conditions for the wave equation. *Math. Comput.* 49 (179), 65–90.
- Hu, F.Q., 2004. Absorbing boundary conditions. *Int. J. Comput. Fluid Dyn.* 18 (6), 513–522.
- Ihlenburg, F., Babuška, I., 1995. Finite element solution of the Helmholtz equation with high wave number Part I: the h-version of the FEM. *Comput. Math. Appl.* 30 (9), 9–37.
- Ihlenburg, F., Babuška, I., 1997. Finite element solution of the Helmholtz equation with high wave number Part II: the hp version of the FEM. *SIAM J. Numer. Anal.* 34 (1), 315–358.
- Ihlenburg, F., Babuška, I., Sauter, S., 1997. Reliability of finite element methods for the numerical computation of waves. *Adv. Eng. Softw.* 28 (7), 417–424.
- Ikuno, H., Yasuura, K., 1978. Numerical calculation of the scattered field from a periodic deformed cylinder using the smoothing process on the mode-matching method. *Radio. Sci.* 13 (6), 937–946.
- Keller, J.B., Givoli, D., 1989. Exact non-reflecting boundary conditions. *J. Comput. Phys.* 82 (1), 172–192.
- Li, E., He, Z.C., Xu, X., Liu, G.R., 2015. Hybrid smoothed finite element method for acoustic problems. *Comput. Meth. Appl. Mech. Eng.* 283, 664–688.
- Li, W., Chai, Y.B., Lei, M., Liu, G.R., 2014a. Analysis of coupled structural-acoustic problems based on the smoothed finite element method (S-FEM). *Eng. Anal. Bound. Elem.* 42 (1), 84–91.
- Li, Y., Li, M., Liu, G.R., 2014b. A modified triangulation algorithm tailored for the smoothed finite element method (S-FEM). *Int. J. Comput. Methods* 11 (01).
- Liu, G.R., Dai, K.Y., Nguyen, T.T., 2007a. A smoothed finite element method for mechanics problems. *Comput. Mech.* 39 (6), 859–877.
- Liu, G.R., Nguyen, T.T., Lam, K.Y., 2007b. Theoretical aspects of the smoothed finite element method (SFEM). *Int. J. Numer. Methods Eng.* 71 (8), 902–930.
- Liu, G.R., Nguyen, T.T., Lam, K.Y., 2009. An edge-based smoothed finite element method (ES-FEM) for static, free and forced vibration analyses of solids. *J. Sound Vib.* 320 (4), 1100–1130.
- Mitri, F.G., 2015a. Acoustic scattering of a cylindrical quasi-Gaussian beam with arbitrary incidence focused on a rigid elliptical cylinder. *J. Appl. Phys.* 118 (18), 184902.
- Mitri, F.G., 2015b. Acoustic radiation force on a rigid elliptical cylinder in plane (quasi) standing waves. *J. Appl. Phys.* 118 (21), 214903.
- Mitri, F.G., 2016. Acoustic backscattering and radiation force on a rigid elliptical cylinder in plane progressive waves. *Ultrasonics* 66, 27–33.
- Nefske, D.J., Wolf, J.A., Howell, L.J., 1982. Structural-acoustic finite element analysis of the automobile passenger compartment: a review of current practice. *J. Sound Vib.* 80 (2), 247–266.
- Petyl, M., Lea, J., Koopmann, G.H., 1976. A finite element method for determining the acoustic modes of irregular shaped cavities. *J. Sound Vib.* 45 (4), 495–502.
- Pillai, T.A.K., Varadan, V.V., Varadan, V.K., 1982. Sound scattering by rigid and elastic infinite elliptical cylinders in water. *J. Acoust. Soc. Am.* 72 (3), 1032–1037.
- Seybert, A.F., Wu, T.W., Wu, X.F., 1988. Radiation and scattering of acoustic waves from elastic solids and shells using the boundary element method. *J. Acoust. Soc. Am.* 84 (5), 1906–1912.
- Strouboulis, T., Hidajat, R., Babuška, I., 2008. The generalized finite element method for Helmholtz equation. Part II: effect of choice of handbook functions, error due to absorbing boundary conditions and its assessment. *Comput. Meth. Appl. Mech. Eng.* 197 (5), 364–380.
- Thompson, L.L., Pinsky, P.M., 1995. A Galerkin least-squares finite element method for the two-dimensional Helmholtz equation. *Int. J. Numer. Methods Eng.* 38 (3), 371–397.
- Turkel, E., Yefet, A., 1998. Absorbing PML boundary layers for wave-like equations. *Appl. Numer. Math.* 27 (4), 533–557.